Effect of light scattering on optical-resolution photoacoustic microscopy

Yan Liu, Chi Zhang, Song Hu, Yuta Suzuki, Zhun Xu, et al.

Yan Liu, Chi Zhang, Song Hu, Yuta Suzuki, Zhun Xu, Silvina Ferradal, Lihong V. Wang, "Effect of light scattering on optical-resolution photoacoustic microscopy," Proc. SPIE 8223, Photons Plus Ultrasound: Imaging and Sensing 2012, 82233S (23 February 2012); doi: 10.1117/12.909373

SPIE.

Event: SPIE BiOS, 2012, San Francisco, California, United States

Effect of Light Scattering on Optical-Resolution Photoacoustic Microscopy

Yan Liu, Chi Zhang, Song Hu, Yuta Suzuki, Zhun Xu, Silvina Ferradal and Lihong V. Wang*

Optical Imaging Laboratory, Department of Biomedical Engineering, Washington University
1 Brookings Drive, Saint Louis, Missouri 63130, USA
*Corresponding author: lhwang@biomed.wustl.edu

ABSTRACT

The penetration depth of ballistic optical imaging technologies is limited by light scattering. To study the effect of scattering on optical-resolution photoacoustic microscopy (OR-PAM), we divided the signals in OR-PAM into two classes: one is from the target volume defined by the optical resolution cell (Class I); the other is from the rest of the acoustic resolution cell (Class II). We developed a way to simulate the point spread function (PSF) of our OR-PAM system considering both optical illumination and acoustic detection, then used the PSF to calculate the contributions of each class of signal to the total signal at different focal depths. Our simulation results showed that: 1) The Class II signal decays much more slowly than the Class I signal; 2) The full width at half maximum (FWHM) of the PSF for the focal depth of 0.9 transport mean free path (TMFP) is not broadened much (~10%) compared with that for a clear medium; 3) Image contrast is degraded with increasing depth when there is a uniform absorption background.

Keywords: Optical-resolution photoacoustic microscopy, light scattering, penetration depth

1. INTRODUCTION

Optical-resolution photoacoustic microscopy (OR-PAM), an emerging label-free optical imaging technology, detects optical absorption contrast with 100% sensitivity. It focuses light into biological tissue and employs an ultrasonic transducer focused on the same region to receive the photoacoustic (PA) signals generated by the absorber. By raster scanning, an image is formed[1].

When imaging biological tissues by using ballistic optical imaging technologies such as confocal microscopy, two photon microscopy and optical coherence tomography (OCT), studies have shown that light scattering will attenuate the signal strength and degrade the image resolution and contrast[2-6]. Thus, the penetration depth of ballistic optical imaging technologies is limited by light scattering. However, to our knowledge, no study on how light scattering affects the performance of OR-PAM has been done. In this paper, we presented our study to address this problem.

2. METHODS

2.1 Two classes of signals in OR-PAM

To study how light scattering degrades the strength and localization of signals, we divided the signals in OR-PAM into two classes. A Class I signal carries information about the absorption property in the target volume, which is defined by the system resolution (See Figure 1):

$$PA_{ClassI}(t, z_f) = \int_{V_I(z_f)} \mu_a(z,\rho) F(z,\rho) Acous(z,\rho,t) dV, \quad (1)$$

while a Class II signal carries information from outside the target volume and obscures the Class I signal:

$$PA_{ClassII}(t, z_f) = \int_{V_{II}(z_f)} \mu_a(z,\rho) F(z,\rho) Acous(z,\rho,t) dV. \quad (2)$$

Photons Plus Ultrasound: Imaging and Sensing 2012, edited by Alexander A. Oraevsky, Lihong V. Wang,
Proc. of SPIE Vol. 8223, 82233S · © 2012 SPIE · CCC code: 1605-7422/12/$18 · doi: 10.1117/12.909373

In Eq.(1) and Eq.(2), we chose cylindrical coordinate systems in the calculation. $\mu_a(z,\rho)$ is the absorption coefficient, $F(z,\rho)$ is the optical fluence, $Acous(z,\rho,t)$ is the PA signal generated by a unit point absorber when $F(z,\rho)=1\,J/m^2$. V_I corresponds to the optical resolution cell, while V_{II} corresponds to the set difference of the acoustic resolution cell and the optical resolution cell. z_f is the focal depth.

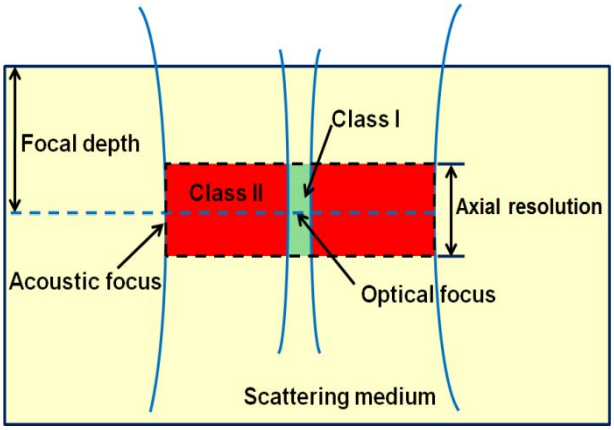

Figure 1. Definition of the Class I and the Class II signal in OR-PAM. The signal generated from the green region (i.e., the optical resolution cell) is the Class I signal, while the signal generated from the red region (i.e., the set difference of the acoustic resolution cell and the optical resolution cell) is the Class II signal.

2.2 Simulation of optical fluence distribution by the Monte Carlo method

We used the Monte Carlo method to calculate the optical fluence distribution in a homogenous scattering medium. Since we were interested in the transverse fluence distribution, we chose the hyperboloid focusing method to simulate optical focusing[7,8]. The traditional geometric focusing method[9] cannot simulate the fluence distribution at the focal plane well because the fluence at the focal point is always much larger than the fluence at the grid points next to the focal point[7] (See Figure 2). The fluence distribution corresponding to each focal depth is the illumination PSF for that depth. The parameters we used in simulations were g=0.9, μ_s=100 cm^{-1}, μ_a=0.1 cm^{-1}, $n_{tissue}=n_{outside\_tissue}$=1.33, numerical aperture (NA) of objective in air =0.1, wavelength of light =570 nm, grid size dr=0.1 μm, dz=1 μm. From the optical properties of the scattering medium, we could get that the TMFP was 1000 μm and the MFP was 100 μm.

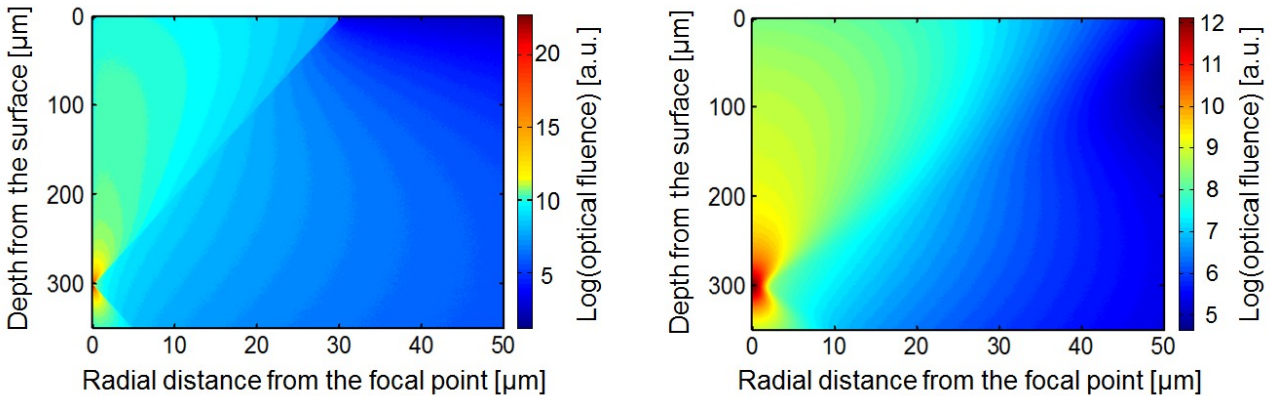

Figure 2. (a) Optical fluence distribution simulated by the traditional geometric focusing method. (b) Optical fluence distribution simulated by the hyperboloid focusing method.

2.3 Simulation of acoustic detection by the impulse response method

OR-PAM employs a high-frequency spherically focused broadband ultrasound transducer to detect PA signals[1]. The detected pressure can be calculated by Eq.(3)[10]:

$$\text{Pressure}(\vec{r}_0;\vec{r}) \propto \mu_a(\vec{r})F(\vec{r})SIR(\vec{r},t) * \delta'\left(t-\frac{|\vec{r}-\vec{r}_0|}{c}\right) * EIR(t), \tag{3}$$

where $\vec{r}_0$ and $\vec{r}$ are the positions of the ultrasound transducer and the PA point source, respectively. $EIR(t)$ is the electro-mechanical impulse response of the transducer and $SIR(\vec{r},t)$ is the spatial impulse response of the transducer, determined by its aperture. $\delta'\left(t-\frac{|\vec{r}-\vec{r}_0|}{c}\right)$ is the PA signal generated by a unit point absorber. $SIR(\vec{r},t) * \delta'\left(t-\frac{|\vec{r}-\vec{r}_0|}{c}\right) * EIR(t)$ is the $Acous(z,\rho,t)$ in Eq.(1) and Eq.(2). $\delta'\left(t-\frac{|\vec{r}-\vec{r}_0|}{c}\right) * EIR(t)$ can be determined experimentally by measuring the PA signal of a point absorber at the focal point[11].

We calculated the $SIR(\vec{r},t)$ of the field points on the focal plane in the frequency domain by using Eq.(4)[12]:

$$SIR(\vec{r},\omega) = uS(e^{-ik|\vec{r}-\vec{r}_0|}/2\pi|\vec{r}-\vec{r}_0|)G(z), \tag{4.1}$$

$$G(z) = (2/z)\sum_{n=0}^{\infty}(-1)^n(h/a)^{2n}J_{2n+1}(z), \tag{4.2}$$

$$z = (1-i/k|\vec{r}-\vec{r}_0|)ka\sin\theta \approx ka\sin\theta, \tag{4.3}$$

where a is the height of the transducer, h is the depth of the concave surface, S is the area of the aperture, u is the normal velocity of the particle on the aperture and θ is the angle between the field point and the axis of the transducer. $k=\frac{\omega}{c}$. The NA of our transducer is 0.46 and its focal length is 4.23 mm, from which we can get a =1.95 mm and h =0.47 mm. Though the author assumes a low NA in the derivation of Eq.(4), Coulouvrat has shown that the formula also applies to the case of a high NA transducer[13].

The magnitude of the calculated $SIR(\vec{r},\omega)$ for three field points on the focal plane is shown in Figure 3. It can be seen that the further the field point from the focal point, the narrower the bandwidth of their $SIR(\vec{r},t)$, and the longer the duration of $SIR(\vec{r},t)$ in the time domain.

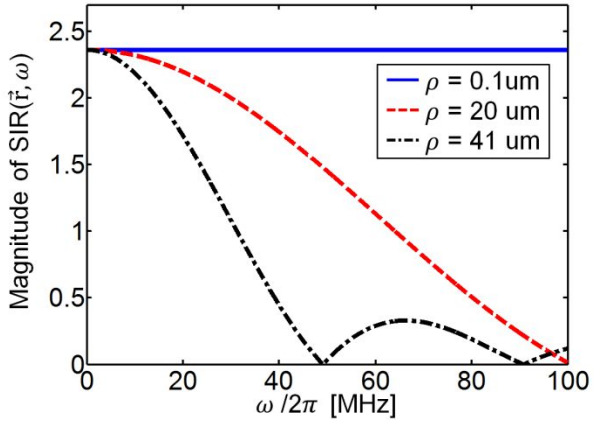

Figure 3. The magnitude of the $SIR(\vec{r},\omega)$ for three field points on the focal plane. ρ is the radial distance between the field point and the focal point.

By using Eq.(3) and setting $\mu_a(\vec{r})F(\vec{r})=1$, the PA signals generated by the same three field points as in Figure 3 are calculated and are shown in Figure 4. It can be seen that the peaks of all three PA signals arrive at the same time. By

extracting the maximum amplitude of the PA signal generated from each field point, a detection PSF can be generated and the detection PSF on the focal plane (detection lateral PSF) is shown in Figure 5. Unlike continuous-wave(CW) detection, there are no sidelobes in the detection lateral PSF for broadband detection. We can also see that the full-width at half maximum (FWHM) of the detection lateral PSF for broadband detection is larger than that for CW detection.

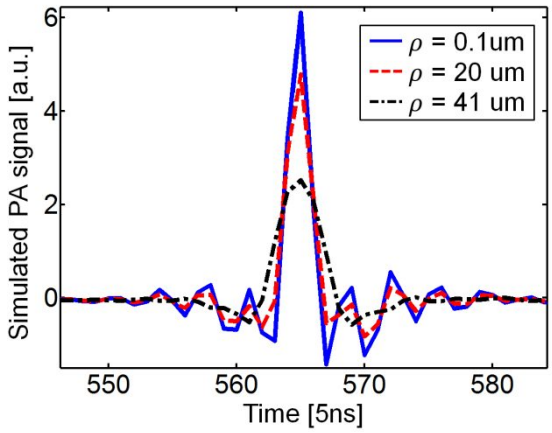

Figure 4. Simulated PA signal for three field points on the focal plane. ρ is the radial distance between the field point and the focal point.

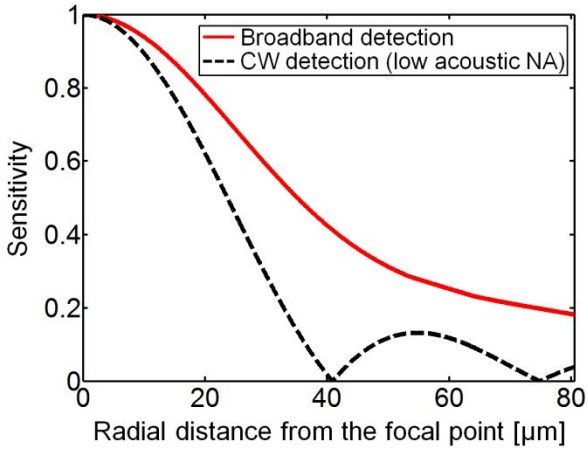

Figure 5. The detection PSF on the focal plane. The red solid curve is for broadband detection. The black dashed curve is for CW detection when a low NA transducer is used.

3. RESULTS

Since the depth of focus of the acoustic focal zone is more than ten times larger than the axial resolution of OR-PAM, we assume that the detection PSF on each depth in the acoustic resolution cell is the same as that on the focal plane. By multiplying the illumination PSF and the detection PSF, a total PSF of OR-PAM is generated. The PSFs on the focal plane for different focal depths are shown in Figure 6. It can be seen that the FWHM of the PSF for focal depth of 0.9 TMFP is not broadened much (about 10%) compared with that for a clear medium, which seems a little unexpected but which agrees with the simulation results by Hayakawa et al.[14]. The shoulder of the PSF rises with increasing depth, due to scattering.

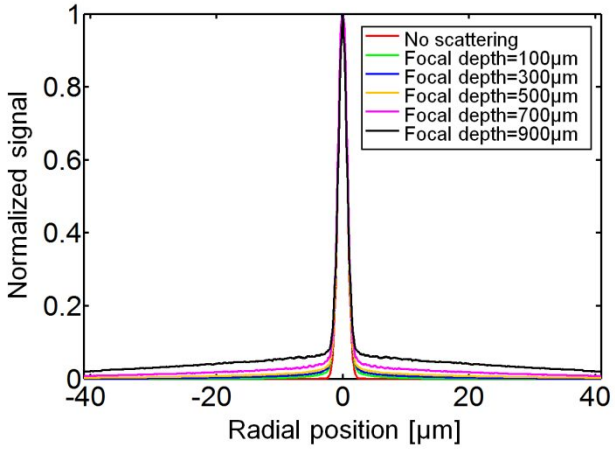

Figure 6. Lateral PSF of OR-PAM for different focal depth.

When we consider a homogenous scattering medium, the peaks of the Class I and the Class II signal at different focal depths can be calculated by using the total PSF and are shown in Figure 7. It can be seen that the Class II signal is stronger than the Class I signal for depths greater than 70 μm (0.7MFP). Thus, image contrast is degraded with increasing depth when there is a uniform absorption background. The signal decay rate of the Class I signal is -9.87 mm^{-1}, whose absolute value is close to μ_t=10.01 mm^{-1}, while the signal decay rate of the Class II signal is -5.28 mm^{-1}, which shows that the Class II signal decays much more slowly than the Class I signal.

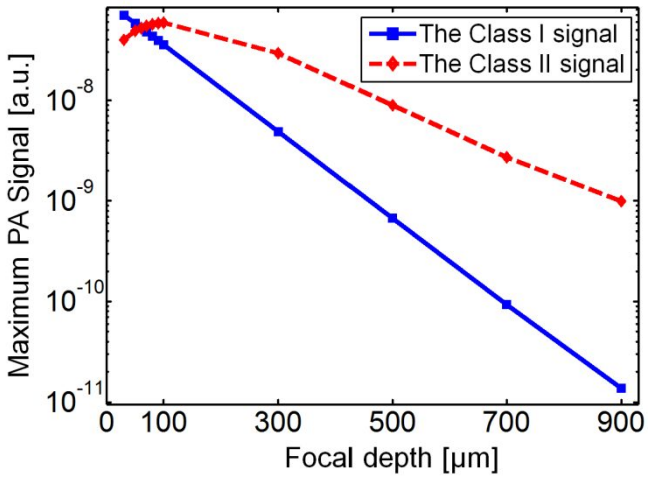

Figure 7. The Class I and the Class II signals at different focal depth.

4. CONCLUTION

We have developed a way to simulate the PSF of the OR-PAM system that considers both optical illumination and acoustic detection. We then used the PSF to calculate the contribution of each class of signal to the total signal for different focal depths. Our simulation showed that: 1) The Class II signal decays much more slowly than the Class I signal; 2) The full width at half maximum (FWHM) of the PSF for the focal depth of 0.9 TMFP is not broadened much (~10%) compared with that for a clear medium; 3) Image contrast is degraded with increasing depth when there is a uniform absorption background. In future, to further study the effect of light scattering, we could use the PSF to simulate the images of other types of objects. We can also study how different system parameters affect the PSF, so as to optimize our system. In addition, the detection PSF calculated in this paper can be approximated as the total PSF of

the acoustic-resolution photoacoustic microscopy[15] (AR-PAM) and therefore can be used to optimize the performance of the AR-PAM system.

ACKNOWLEDGEMENT

We would like to thank Zijian Guo and Kun Wang for helpful discussions. This work was sponsored in part by National Institutes of Health grants R01 EB008085, R01 EB000712, R01 CA134539, R01 CA157277, and U54 CA 136398. L. W. has a financial interest in Microphotoacoustics, Inc. and Endra, Inc., which, however, did not support this work.

REFERENCES

[1] K. Maslov, H. F. Zhang, S. Hu, and L. V. Wang, "Optical-resolution photoacoustic microscopy for in vivo imaging of single capillaries," Opt. Lett. 33(9), 929-931 (2008).
[2] J. M. Schmitt, A. Knüttel, and M. Yadlowsky, "Confocal microscopy in turbid media," J. Opt. Soc. Am. A 11, 2226-2235 (1994).
[3] N. J. Durr, C.T. Weisspfennig, B.A. Holfeld and A. Ben-Yakar, "Maximum imaging depth of two-photon autofluorescence microscopy in epithelial tissues," J Biomed Opt 16 (2) , 026008 (2011).
[4] D. J. Smithies, T. Lindmo, Z. Chen, J. S. Nelson and T. E. Milner, "Signal attenuation and localization in optical coherence tomography studied by Monte Carlo simulation," Phys. Med. Biol. 43(10), 3025-3044 (1998).
[5] R. Wang, "Signal degradation by multiple scattering in optical coherence tomography of dense tissue: a Monte Carlo study towards optical clearing of biotissues," Phys. Med. Biol. 47(13), 2281–2299 (2002).
[6] G. Yao and L. V. Wang, "Monte Carlo simulation of an optical coherence tomography signal in homogeneous turbid media," Phys. Med. Biol. 44(9), 2307-2320(1999).
[7] A. Tycho, T. M. Jørgensen, H. T. Yura, and P. E. Andersen, "Derivation of a Monte Carlo method for modeling heterodyne detection in optical coherence tomography systems," Appl. Opt. 41, 6676-6691 (2002).
[8] F. Zhang, M. Kinnunen, A.Popov and R. Myllylä, "Monte Carlo method for simulating optical coherence tomography signal in homogeneous turbid media," Proc. SPIE 7022, 702213 (2001).
[9] L. V. Wang and G. Liang, "Absorption distribution of an optical beam focused into a turbid medium," Appl. Opt. 38, 4951-4958 (1999)
[10] K. Wang, S. A. Ermilov, R. Su, H. Brecht, A. A. Oraevsky and M. A. Anastasio, "An imaging model incorporating ultrasonic transducer properties for three-dimensional optoacoustic tomography," IEEE Trans. Med. Imaging 30(2), 203-214,(2011)
[11] M. Arditi, F. S. Foster and J. W. Hunt, "Transient fields of concave annular arrays," Ultrasonic Imaging 3, 37-61 (1981).
[12] H. T. O'Neil, "Theory of focusing radiators," J. Acoust. Soc. Am. 21(5), 516-526 (1949)
[13] François Coulouvrat, "Continuous field radiated by a geometrically focused transducer: numerical investigation and comparison with an approximate model," J. Acoust. Soc. Am. 94 (3), 1663-1675 (1993)
[14] C. K. Hayakawa, V. Venugopalan, V. V. Krishnamachari and E. O. Potma, "Amplitude and phase of tightly focused laser beams in turbid media," Phys. Rev. Lett. 103(4), 043903 (2009).
[15] H. F. Zhang, K. Maslov, G. Stoica and L. H. V. Wang, "Functional photoacoustic microscopy for high-resolution and noninvasive in vivo imaging," Nat. Biotechnol. 24(7), 848-851 (2006)